

MOLECULAR LINE EMISSION FROM A PROTOPLANETARY DISK IRRADIATED EXTERNALLY BY A NEARBY MASSIVE STAR

Catherine Walsh^{1,2}, T. J. Millar¹, & Hideko Nomura³

`cwalsh@strw.leidenuniv.nl`

Received 2012 December 28; accepted 2013 March 4

¹Astrophysics Research Centre, School of Mathematics and Physics, Queen's University Belfast, University Road, Belfast BT7 1NN, UK

²Leiden Observatory, Leiden University, P.O. Box 9513, NL-2300 RA Leiden, The Netherlands

³Department of Astronomy, Graduate School of Science, Kyoto University, Kyoto 606-8502, Japan

ABSTRACT

Star formation often occurs within or nearby stellar clusters. Irradiation by nearby massive stars can photoevaporate protoplanetary disks around young stars (so-called proplyds) which raises questions regarding the ability of planet formation to take place in these environments. We investigate the two-dimensional physical and chemical structure of a protoplanetary disk surrounding a low-mass (T Tauri) star which is irradiated by a nearby massive O-type star to determine the survivability and observability of molecules in proplyds. Compared with an isolated star-disk system, the gas temperature ranges from a factor of a few (in the disk midplane) to around two orders of magnitude (in the disk surface) higher in the irradiated disk. Although the UV flux in the outer disk, in particular, is several orders of magnitude higher, the surface density of the disk is sufficient for effective shielding of the disk midplane so that the disk remains predominantly molecular in nature. We also find that non-volatile molecules, such as HCN and H₂O, are able to freeze out onto dust grains in the disk midplane so that the formation of icy planetesimals, e.g., comets, may also be possible in proplyds. We have calculated the molecular line emission from the disk assuming LTE and determined that multiple transitions of atomic carbon, CO (and isotopologues, ¹³CO and C¹⁸O), HCO⁺, CN, and HCN may be observable with ALMA, allowing characterization of the gas column density, temperature, and optical depth in proplyds at the distance of Orion (≈ 400 pc).

Subject headings: astrochemistry — line: profiles — protoplanetary disks — stars: formation

1. INTRODUCTION

Star formation rarely takes place in isolation; stars form primarily within multiple systems and often within, or nearby, massive stellar clusters (see, e.g., Kennicutt & Evans 2012). Thus, the young star’s protoplanetary disk can be heavily irradiated and indeed, photoevaporated, by nearby massive stars (see, e.g., Bally et al. 1998), for example, the famous *proplyds* in the Orion nebula (O’Dell et al. 1993). The properties of proplyds have been well studied since their discovery; however, little is known about their molecular content due to their small size ($R \sim 100\text{--}1000$ AU) and relatively large distance, e.g., Orion at ≈ 400 pc. Protoplanetary disks are the sites of planet formation and the study of disks in extreme environments is important for a complete understanding of this process. Can the disk survive sufficiently long for planet formation to take place? This has implications on our understanding of the formation of our own solar system as it is thought that the Sun formed within a stellar cluster which has long since dispersed (see, e.g., Adams 2010, and references therein).

We calculate the chemical structure and molecular line emission from a protoplanetary disk around a classical T Tauri star which is irradiated by a nearby ($\lesssim 0.1$ pc) massive O-type star. Our aims are (1) to determine whether molecules are able to form and survive in the disk, (2) to identify species which may be observable with ALMA, and (3) to identify species which can characterize the physical conditions and the subsequent implications on planet formation.

2. PROTOPLANETARY DISK MODEL

2.1. Physical Model

We model a steady axisymmetric disk in Keplerian rotation about a classical T Tauri star with mass $0.5 M_{\odot}$, radius $2 R_{\odot}$, effective temperature 4000 K, and $\alpha = 0.01$, using the methods outlined in Nomura & Millar (2005) and Nomura et al. (2007). The radial surface density distribution is determined assuming a constant mass accretion rate, $\dot{M} = 10^{-8} M_{\odot} \text{ yr}^{-1}$ (Pringle 1981). To determine the density and temperature structure, we solve the equation of hydrostatic equilibrium in the vertical direction and the local thermal balance between the heating and cooling of the gas. We include grain photoelectric heating by UV photons and heating via hydrogen ionization by X-rays and allow the gas to cool via gas–grain collisions and line transitions.

Our disk is irradiated by UV photons and X-rays from the central star and UV photons from the interstellar radiation field and a nearby massive O-type star. We model the UV spectrum of the O-type star as a blackbody with an effective temperature of 45,000 K. We set the UV flux at the disk surface to $(4 \times 10^5) \times G_0$, where $G_0 \approx 1.6 \times 10^{-3} \text{ erg cm}^{-2} \text{ s}^{-1}$ is the average strength of the integrated interstellar radiation field. This corresponds to a distance between the disk and the massive star of $\lesssim 0.1 \text{ pc}$.

We assume the dust and the gas in the disk are well mixed and adopt a dust–grain size distribution which reproduces the extinction curve observed in dense clouds (Weingartner & Draine 2001). We note that this is a simplistic treatment of the dust distribution in disks since it is thought that gravitational dust settling and coagulation perturb the dust size and density distribution from that observed in dense clouds (see, e.g., Dullemond & Dominik 2004; D’Alessio et al. 2006).

2.2. Chemical Model

We use the gas–grain chemical network from Walsh et al. (2010) and compute the photoreaction rates and X-ray ionization rates using the methods outlined in Walsh et al. (2012). Our gas-phase chemistry is from the UMIST Database for Astrochemistry (Woodall et al. 2007). We include freezeout of gas-phase material onto dust grains and thermal and non-thermal desorption. We allow photodesorption by both external and internal UV photons and desorption via cosmic-ray heating of dust grains (Hasegawa & Herbst 1993; Öberg et al. 2009a,b). We use a small grain-surface network to include the synthesis of several complex organic molecules, e.g., methanol (Hasegawa et al. 1992; Hasegawa & Herbst 1993). We include the photodestruction of grain mantle material by UV photons, X-rays, and cosmic rays (Ruffle & Herbst 2001). Experiments have shown that the irradiation of interstellar ice analogs by UV and X-ray photons induces chemistry in the ice (see, e.g., Hagen et al. 1979; D’Hendecourt et al. 1986; Allamandola et al. 1988; Öberg et al. 2010b; Ciaravella et al. 2010). We adopt the equivalent gas-phase photorates for ice species and allow the products to remain on the grain to take part in further grain-surface reactions.

We assume the grains are negatively charged compact spheres with a radius of $0.1 \mu\text{m}$ and a constant fractional abundance of $\sim 10^{-12}$ relative to the gas number density, equivalent to a gas-to-dust mass ratio of ~ 100 . We adopt a sticking coefficient, $S \approx 1$, for all species. We include the dissociative recombination of gas-phase cations with dust grains. The dust model used for the chemistry is simple compared with that used to calculate the disk physical structure; however, the total dust-grain cross section is consistent between models.

Our initial abundances are from the output of a dark cloud model at an age of $\sim 10^5$ yr. Our underlying elemental abundance ratios for H:He:C:N:O:Na:Mg:Si:S:Cl:Fe are 1.00:0.14:7.30(−5):2.14(−5):1.76(−4):3.00(−9):3.00(−9):3.00(−9):2.00(−8):3.00(−9):3.00(−9).

We map the chemical structure of the disk at a time of 10^6 yr, the typical age of classical T Tauri stars.

2.3. Molecular Line Emission

To estimate the molecular line emission, we assume the disk is “face on” and that local thermodynamic equilibrium (LTE) holds throughout. We calculate the emergent flux from the top (i.e., visible) half of the disk only which we also assume is the surface directly irradiated by the nearby massive star. In reality, the lower half, although not directly irradiated by the nearby star, is subject to diffuse, scattered UV radiation originating from the stellar cluster, and this needs to be taken into account in the calculation of the physical structure of the lower disk. Hence, our estimated molecular line emission strengths are *lower limits* to the potentially observable line strengths. We include only thermal broadening of the line profiles because this will dominate turbulent broadening. For CO isotopologues, we assume the molecular isotopic ratios reflect the atomic ratios and use values applicable for the local interstellar medium: $^{13}\text{C}/^{12}\text{C} = 1/77$ and $^{18}\text{O}/^{16}\text{O} = 1/560$ (Wilson & Rood 1994).

3. RESULTS

3.1. Physical Structure

In Figure 1, we present the gas temperature, number density, integrated UV flux, and integrated X-ray flux as a function of disk radius, R , and height, Z/R . We also display these parameters, along with the cosmic-ray and X-ray ionization rates, as a function of height at $R = 100$ AU. We compare results from our irradiated disk (solid lines) and isolated disk (dashed lines; see Walsh et al. 2012). Here, “irradiated” refers to a disk irradiated by a

nearby massive star *and* the central star, whereas, “isolated” refers to a disk irradiated by the central star *only*.

Compared with the isolated disk, the gas and dust temperatures in the irradiated disk are significantly higher in the outer disk midplane ($R \gtrsim 1$ AU). The gas temperature structure in the innermost region, $R \lesssim 1$ AU, is similar in both disks because this is driven by irradiation by the central star. The density structure is also perturbed, depending on the gas temperature profile.

In the surface at 100 AU, we see around an order of magnitude decrease in the X-ray flux and subsequent ionization rate in the irradiated model, compared with the isolated model. This is due to the differing attenuation of X-rays along the line of sight from the central star, which is affected by the density and gas temperature profile in the disk. In the disk midplane, the X-ray flux (and ionization rate) is similar in both models. We see a large increase in the UV flux in the disk surface, increasing from a value of $\sim 1 \text{ erg cm}^{-2} \text{ s}^{-1}$ in the isolated case to $\sim 100 \text{ erg cm}^{-2} \text{ s}^{-1}$ in the irradiated case at $R = 100$ AU. The surface density in the irradiated disk is sufficient for the disk midplane to remain effectively shielded from all sources of UV irradiation.

3.2. Chemical Structure

In Figure 2, we present the fractional abundance (relative to number density) of gas-phase CO, HCO^+ , CN, HCN, C_2H , CS, H_2CO and N_2H^+ as a function of disk radius, R , and height, R/Z . These species have been detected in numerous nearby gas-rich primordial isolated protoplanetary disks due their relatively large abundance and simple rotational spectra leading to strong emission lines (see, e.g., Thi et al. 2004; Dutrey et al. 2007; Henning et al. 2010; Öberg et al. 2010a; Dutrey et al. 2011). In Figure 3, we present

the vertical column densities as a function of disk radius, R . We have smoothed the column densities using a Bézier function of index, n , where n is the number of data points. We also present the column densities for those additional species observed in protoplanetary disks in absorption and/or emission at infrared wavelengths: OH, H₂O, C₂H₂, and CO₂ (bottom, see, e.g., Lahuis et al. 2006; Carr & Najita 2008; Mandell et al. 2012). We also show the grain-surface column densities (dashed lines) for species which exhibit significant freezeout. In Table 1, we list the calculated column densities at radii of 10 AU and 100 AU.

We see a different chemical stratification in the irradiated disk, compared with the isolated disk. The higher dust temperature in the disk midplane allows volatile molecules, such as CO, to remain in the gas, whereas tightly bound molecules, such as HCN, freeze onto grain surfaces. Instead of the usual “warm molecular layer” observed between $0.3 \lesssim Z/R \lesssim 0.5$, we see a thinner molecular layer which is deeper in the disk and abundant in radicals, e.g., CN, C₂H, and CS, and molecules. HCO⁺ resides in a layer slightly higher than the “molecule/radical” layer reflecting the abundance of proton-donating molecules, such as, H₃⁺ and H₃O⁺.

Gas-phase CO possesses its canonical fractional abundance of 10^{-4} throughout the disk midplane and also survives in the disk surface beyond $R \gtrsim 10$ AU with a fractional abundance, $\sim 10^{-7}$. Thus, the disk remains significantly molecular in nature, even under extreme irradiation. We see hints of the truncation of the molecular disk beyond ≈ 50 AU. Here, we have assumed hydrostatic equilibrium, whereas, in reality, photoevaporative flow may affect the surface density of the outer disk. The disk truncation radius depends primarily on the scale of the flow (see, e.g., Adams et al. 2004).

HCN is depleted in the disk midplane due to freezeout and reaches a fractional abundance of $\sim 10^{-7}$ in the “molecule/radical” layer beyond $R = 1$ AU. Within this radius, thermal desorption from dust grains increases the fractional abundance to $\sim 10^{-4}$. HCO⁺

and CN both reach a fractional abundance of $\sim 10^{-6}$, whereas C₂H and CS reach a value of $\sim 10^{-7}$. H₂CO and N₂H⁺ reach lower peak values of $\sim 10^{-8}$ and $\sim 10^{-9}$, respectively. N₂H⁺ reaches this value within a radius $\lesssim 1$ AU only.

Comparing column densities at 10 AU, there are minor differences between models (less than a factor of three) for most species. However, in the irradiated disk, the CN, CS, and CO₂ column densities are larger, by factors of 4.7, 44, and 1800, respectively, and those for N₂H⁺, H₂O, and C₂H₂, are smaller, by factors of 9.6, 7.0, and 9.6, respectively. The CN/HCN, OH/H₂O, C₂H/C₂H₂ column density ratios are also larger in the irradiated disk, 1.9, 2.9, and 8.2 versus 0.16, 0.26, and 0.29, respectively, indicative of increased photodissociation of HCN, H₂O, and C₂H₂. Both models exhibit peaks in the CS column density where the dust temperatures are comparable (10 AU in the irradiated disk and 4-5 AU in the isolated disk.) Hence, freezeout onto dust grains accounts for the difference in the CS column densities at 10 AU. The CO₂ column density is significantly larger in the irradiated disk $\approx 2 \times 10^{19}$ cm⁻² versus $\sim 10^{16}$ cm⁻². In the isolated disk, the snow line for CO₂ lies within 10 AU; however, in the irradiated disk, the temperature in the midplane at 10 AU, and beyond, is high enough for CO₂ to possess a significant gas-phase abundance.

At 100 AU, the effects of external irradiation are clear. The H/H₂ column density ratio is much larger in the irradiated disk, 2.9×10^{-2} versus 6.5×10^{-5} for the isolated disk. The OH/H₂O and C₂H/C₂H₂ column density ratios are also larger, 3.3 and 7.0 versus 0.20 and 0.47, respectively. The OH and H₂O column densities also increase significantly in the irradiated disk, by factors of 94 and 5.8, respectively. OH and H₂O can form efficiently in warm/hot gas ($T \gtrsim 200$ K) via the reactions, H₂ + O and H₂ + OH (Glassgold et al. 2009). The HCO⁺ column density is a factor of 6.3 larger in the irradiated disk, tracing the increased ionization degree. We see only minor differences in the column densities of all other species, except CO₂ (already discussed) and N₂H⁺, the latter of which is a factor of

35 smaller in the irradiated disk, at 100 AU. N_2H^+ is destroyed via reactions with CO and electrons. The CO abundance in both models is similar; however, the electron abundance in the molecular layer of the irradiated model is several orders of magnitude higher so that N_2H^+ destruction via dissociative recombination is more effective in this model.

The best astrophysical analog of our isolated disk model is TW Hya. We achieve good agreement with the disk-averaged abundance ratios for CN/HCN derived by Thi et al. (2004, 7.1 versus 3.8 in our model) and the fractional abundance of water vapor determined by Hogerheijde et al. (2011, $5\text{--}20 \times 10^{-8}$ versus $1\text{--}3 \times 10^{-8}$). Adjusting for source size and distance, we achieve reasonable agreement with H_2CO line strengths observed by Qi et al. (2013): 1.22 and 0.54 Jy km s $^{-1}$ versus 0.65 and 0.82 Jy km s $^{-1}$ from our model for the $4_{14}\text{--}3_{13}$ and $5_{15}\text{--}4_{14}$ transitions, respectively (C. Walsh et al., in preparation). We get poor agreement for the HCO^+/CO ratio from Thi et al. (2004, 1.4×10^{-4} versus 2.5×10^{-6}) and our N_2H^+ line strengths are around an order of magnitude lower than that observed. The truncation of our disk at 100 AU means we do not account for the depletion of CO onto dust grains at larger radii where $T_{\text{dust}} \lesssim 20$ K. As discussed previously, N_2H^+ is destroyed via reaction with CO.

3.3. Molecular Line Emission

In Figure 4, we present our synthetic line spectra in ALMA receiver bands 6–9. We assume a maximum disk radius of 100 AU and a distance to source of 400 pc. The lines in bands 3 and 4 are likely too weak to be observable and observations in band 10 are difficult due to increased atmospheric absorption at higher frequencies. Due primarily to the higher gas temperature, the emission lines from the irradiated disk reach higher *peak* values than the equivalent lines from the isolated disk. This is most notable for C, CO (and isotopologues), CN, CS, and HCN. The HCO^+ transitions in bands 6 and 7 reach higher

peak flux densities in the isolated disk and are also much stronger than those for HCN, despite both molecules possessing similar rotational spectra. HCO^+ is a tracer of cold, dense material and is generally more abundant than HCN in the outer disk midplane.

In Table 1, we list the transitions, frequencies, and integrated line intensities. Due to the higher gas temperature in the irradiated disk ($\gg 50$ K), lower frequency transitions ($\nu \sim 100$ GHz) are weaker than higher frequency transitions and the integrated line strengths are stronger than those for the isolated disk. A significant proportion of the CO, ^{13}CO , and C^{18}O ladders should be observable with ALMA advantageously allowing characterization of the gas excitation temperature, column density, and optical depth (see, e.g., Bruderer et al. 2012). Multiple transitions of CI, HCO^+ , HCN, and CN may also be observable allowing additional characterization of the physical conditions. The CN/HCN and CI/CO line ratios and derived column densities would also allow a measurement of the degree of photodestruction in the disk. The remaining molecules would be difficult to observe; however, CS and C_2H may be observable in larger, more massive, proplyds ($100 \text{ AU} \ll R \lesssim 400 \text{ AU}$).

4. DISCUSSION

Proplyds have been extensively studied since their discovery (see, e.g., O’Dell et al. 1993; Bally et al. 1998), and were originally observed in silhouette against the bright nebular background. Early models concentrated on characterizing physical properties: morphology, surface density, mass, dust distribution, mass-loss rates, and lifetime (see, e.g., Johnstone et al. 1998; Störzer & Hollenbach 1999; Richling & Yorke 2000; Adams et al. 2004; Clarke 2007). Models generally agree that the disk survives for a few Myr, beyond which, photoevaporation destroys the disk on a timescale $\sim 10^5$ yr, depending on the distance from the massive star. In Figure 1, we identify the region where the gas temperature equals

the critical temperature for photoevaporation, i.e., where the photoevaporative flow likely originates. According to Dullemond et al. (2007), $T_{\text{crit}} \approx 0.2 T_{\text{virial}}$, where T_{virial} is the temperature at which the sound speed equals the escape velocity of the gas. Several groups (e.g., Adams et al. 2004) model the disk as a photon-dominated region (PDR) including a small chemical network for the computation of the thermal balance and do not report the molecular structure beyond the transition from atomic to molecular hydrogen. Other authors report chemical structure calculations and resulting line emission; however, this has been restricted to ionic and atomic lines (see, e.g., Richling & Yorke 2000). Nguyen et al. (2002) studied the chemistry in irradiated disks around high-mass and low-mass stars, modeling the disk structure as a series of one-dimensional vertical PDRs. They categorize “observable” molecules as those possessing a value $\geq 10^{12} \text{ cm}^{-2}$. In their low-mass model, their column densities for HCN, H_2CO , H_2O , and C_2H are larger than ours by more than an order of magnitude despite both models generating similar CO column densities. We find the opposite case for HCO^+ and CN. These differences likely arise from different prescriptions for the disk structure: we perform a self-consistent calculation of the physical structure, whereas Nguyen et al. (2002) adopt assumed conditions. Our work highlights the importance of radiative transfer calculations in determining the potential observability of molecules, rather than relying on column density calculations.

Here, we report the results of a self-consistent two-dimensional model of the physical and chemical structure of a protoplanetary disk irradiated by a nearby massive star. The disk remains predominantly molecular in nature over the lifetime of the disk ($\approx 10^6 \text{ yr}$) with potentially observable abundances of atoms and molecules (C, CO, HCO^+ , CN, and HCN) at (sub)mm wavelengths. The disk midplane is effectively shielded from UV radiation such that non-volatile molecules, e.g., HCN and H_2O , are frozen out onto dust grains suggesting icy planetesimal formation may be possible in protoplanetary disks. Observations of multiple transitions of these species (and isotopologues) would allow characterization of the

gas surface density, excitation temperature, and optical depth. As far as we are aware, the work reported here is the first attempt to model the two-dimensional molecular structure and resultant (sub)mm molecular line emission of a proplyd.

Astrophysics at QUB is supported by a grant from the STFC. H. Nomura acknowledges the Grant-in-Aid for Scientific Research 21740137, 23103005 and the Global COE Program “The Next Generation of Physics, Spun from Universality and Emergence” from MEXT, Japan.

REFERENCES

- Adams, F. C. 2010, *ARA&A*, 48, 47
- Adams, F. C., Hollenbach, D., Laughlin, G., & Gorti, U. 2004, *ApJ*, 611, 360
- Allamandola, L. J., Sandford, S. A., & Valero, G. J. 1988, *Icar*, 76, 225
- Bally, J., Sutherland, R. S., Devine, D., & Johnstone, D. 1998, *AJ*, 116, 293
- Bruderer, S., van Dishoeck, E. F., Doty, S. D., & Herczeg, G. J. 2012, *A&A*, 541, A91
- Carr, J. S. & Najita, J. R. 2008, *Sci*, 319, 1504
- Ciaravella, A., Muñoz Caro, G., Jiménez Escobar, A., et al. 2010, *ApJL*, 722, L45
- Clarke, C. J. 2007, *MNRAS*, 376, 1350
- D’Alessio, P., Calvet, N., Hartmann, L., Franco-Hernández, R., & Servín, H. 2006, *ApJ*, 638, 314
- D’Hendecourt, L. B., Allamandola, L. J., Grim. R. J. A., & Greenberg, J. M. 1986 *A&A*, 158 119
- Dullemond, C. P. & Dominik, C. 2004, *A&A*, 421, 1075
- Dullemond, C. P., Hollenbach, D., Kamp, I., & D’Alessio, P. 2007, in *Protostars and Planets V*, ed. B. Reipurth, D. Jewitt, K. Keil (Tucson, AZ: Univ. Arizona Press), 555
- Dutrey, A., Henning, T., Guilloteau, S., et al. 2007, *A&A*, 464, 615
- Dutrey, A., Wakelam, V., Boehler, Y., et al. 2011, *A&A*, 535, A104
- Glassgold, A. E., Meijerink, R., & Najita, J. R. 2009, *ApJ*, 701, 142
- Hagen, W., Allamandola, L. J., & Greenberg, J. M. 1979, *Ap&SS*, 65, 215

- Hasegawa, T. I. & Herbst, E. 1993, MNRAS, 261, 83
- Hasegawa, T. I., Herbst, E., & Leung, C. M. 1992, ApJS, 82, 167
- Henning, Th., Semenov, D., Guilloteau, St., et al. 2010, ApJ, 714, 1511
- Hogerheijde, M. R., Bergin, E. A., Brinch, C., et al. 2011, Sci, 334, 338
- Johnstone, D., Hollenbach, D., & Bally, J. 1998, ApJ, 499, 758
- Kennicutt, R. C., Jr. & Evans, N. J., II 2012, ARA&A, 50, 531
- Lahuis, F., van Dishoeck, E. F., Boogert, A. C. A., et al. 2006, ApJL, 636, L145
- Mandell, A. M., Bast, J., van Dishoeck, E. F., et al. 2012, ApJ, 747, 92
- Nomura, H., Aikawa, Y., Tsujimoto, M., Nakagawa, Y., & Millar, T. J. 2007, ApJ, 661, 334
- Nomura, H. & Millar, T. J. 2005, A&A, 438, 923
- Nguyen, T. K., Viti, S., & Williams, D. A. 2002, A&A, 387, 1083
- Öberg, K. I., Linnartz, H., Visser, R., & van Dishoeck, E. F. 2009a, ApJ, 693, 1209
- Öberg, K. I., Qi, C., Fogel, J. K. J. 2010a, ApJ, 720, 480
- Öberg, K. I., van Dishoeck, E. F., & Linnartz, H. 2009b, A&A, 496, 281
- Öberg, K. I., van Dishoeck, E. F., Linnartz, H., & Andersson, S. 2010b, ApJ, 718, 832
- O’Dell, C. R., Wen, Z., & Hu, X. 1993, ApJ, 410, 696
- Pringle, J. E. 1981, ARA&A, 19, 137
- Qi, C., Öberg, K. I., & Wilner, D. J. 2013, ApJ, 765, 34
- Richling, S. & Yorke, H. W. 2000, ApJ, 539, 258

- Ruffle, D. P. & Herbst, E. 2001, MNRAS, 322, 770
- Störzer, H. & Hollenbach, D. 1999, ApJ, 515, 669
- Thi, W.-F., van Zadelhoff, G.-J., & van Dishoeck, E. F. 2004, A&A, 425, 955
- Walsh, C., Millar, T. J., & Nomura, H. 2010, ApJ, 722, 1607
- Walsh, C., Nomura, H., Millar, T. J., & Aikawa, Y. 2012, ApJ, 747, 114
- Weingartner, J. C. & Draine, B. T. 2001, ApJ, 548, 296
- Wilson, T. L. & Rood, R. T. 1994, ARA&A, 32, 191
- Woodall, J., Agúndez, M., Markwick-Kemper, A. J., & Millar, T. J. 2007, A&A, 466, 1197

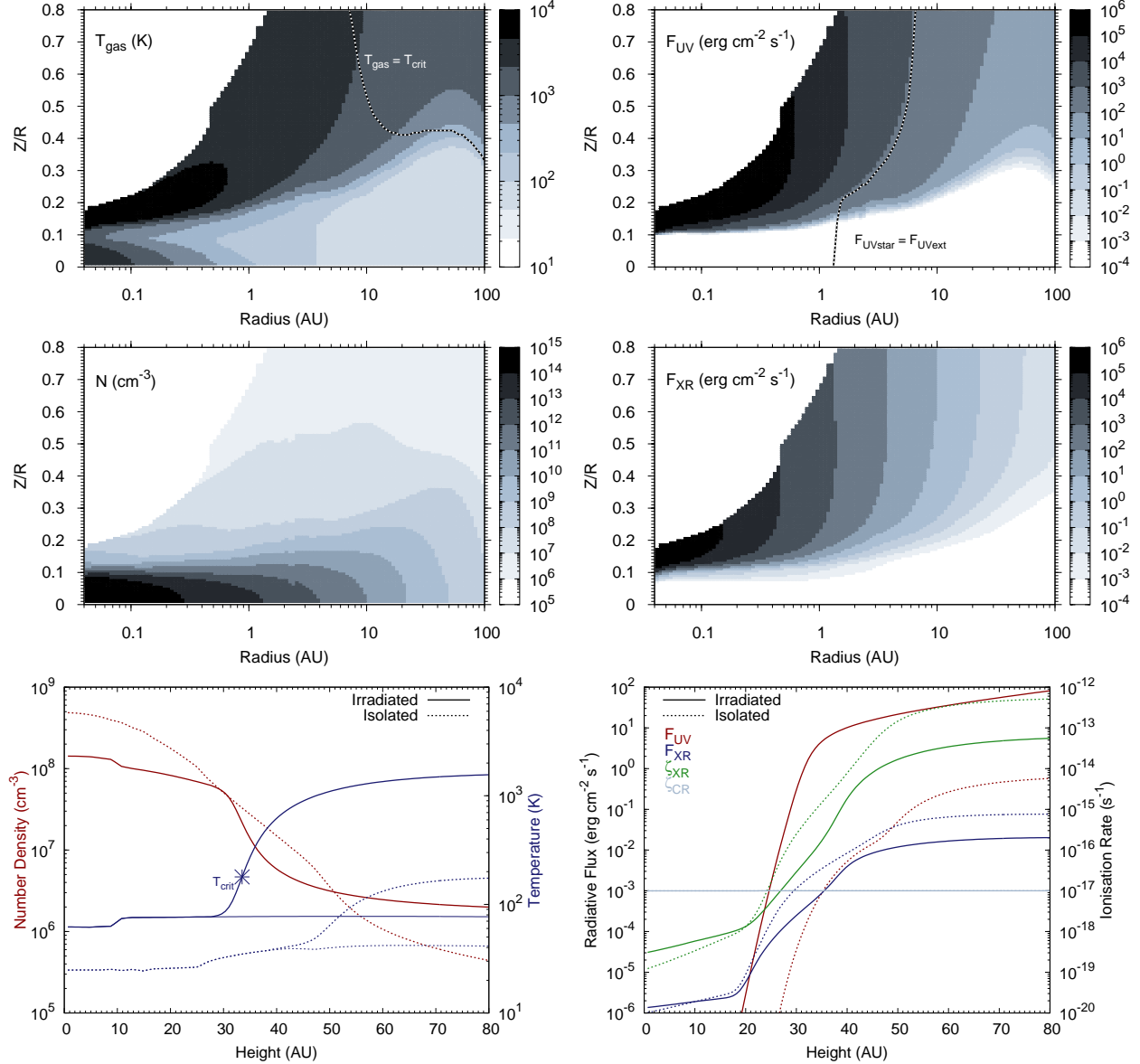


Fig. 1.— Gas temperature, number density, UV flux and X-ray flux as a function of disk radius, R , and height, Z/R (top two rows). Gas and dust temperature, number density, UV flux, X-ray flux, X-ray ionization rate, and cosmic-ray ionization rate as a function of height, Z , at a radius of 100 AU (bottom row), for an irradiated disk (solid lines) and an isolated disk (dashed lines). The lines in the top left and right panels identify where the gas temperature equals the critical temperature for photoevaporation, T_{crit} , and where the contribution to the UV field strength from the central star equals that from the external star.

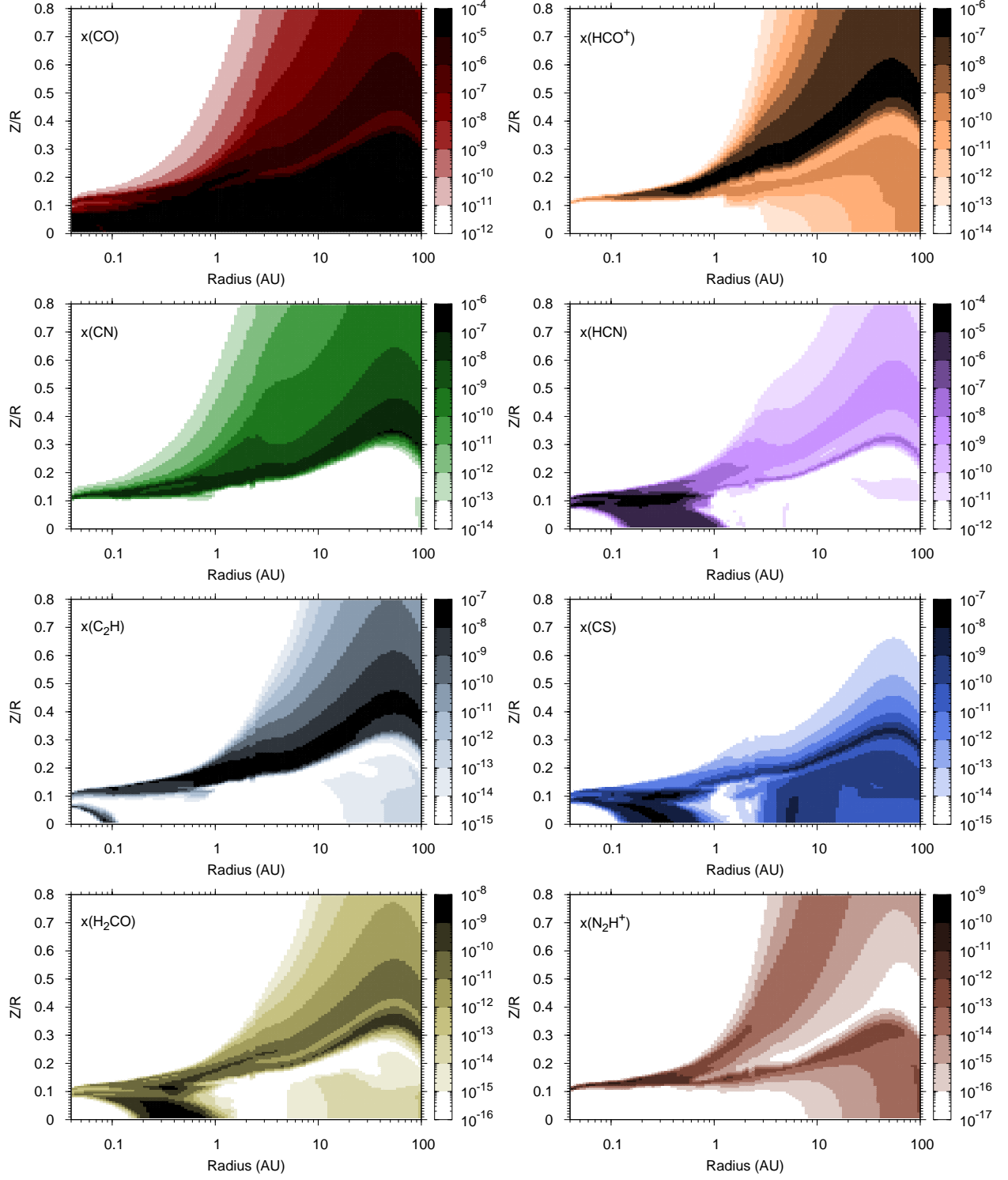


Fig. 2.— Fractional abundance of molecules (relative to number density) as a function of disk radius, R , and height, Z/R .

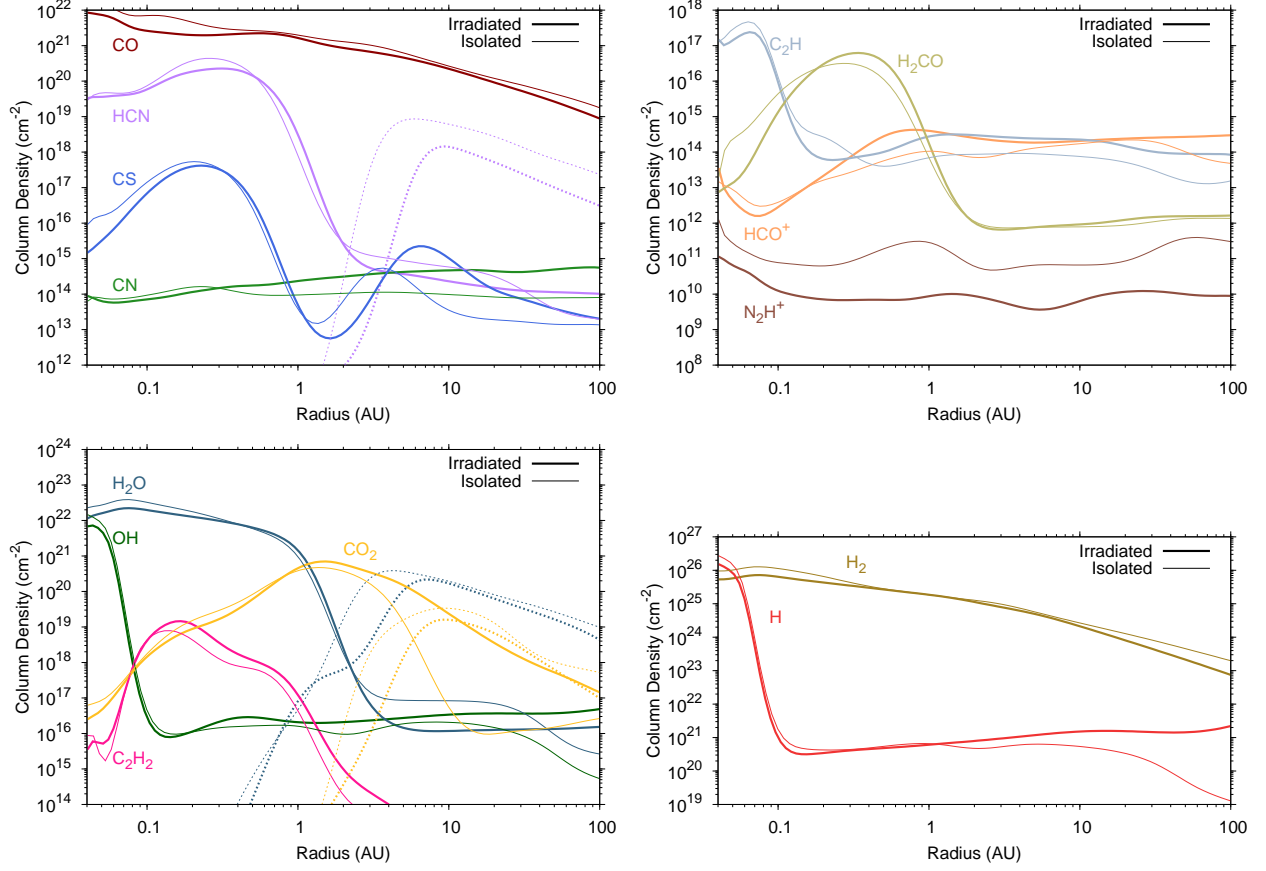


Fig. 3.— Vertical column densities of species as a function of disk radius, R , for an irradiated disk (thick lines) and an isolated disk (thin lines). The grain-surface (ice) column densities are represented by the dashed lines.

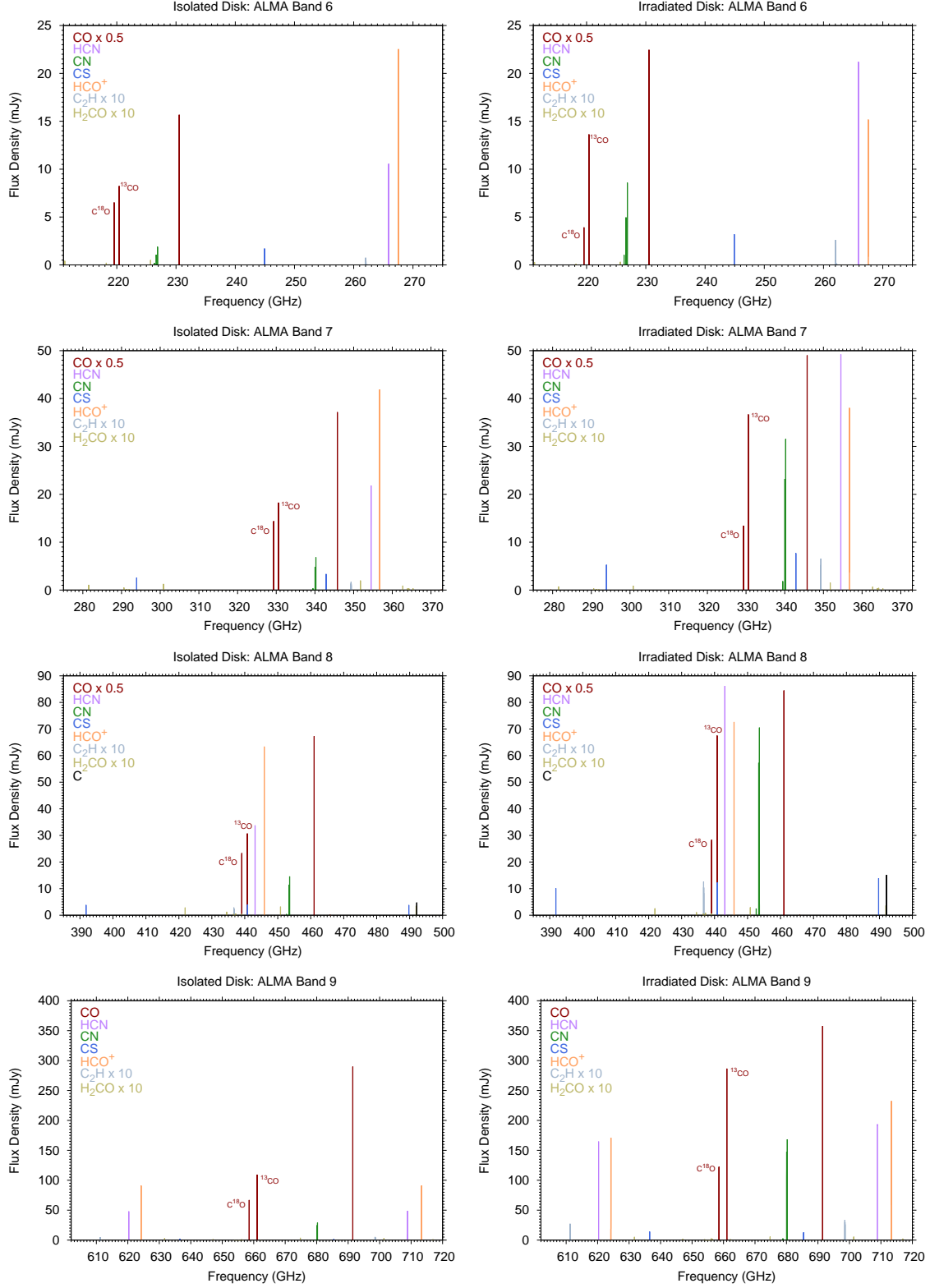


Fig. 4.— Synthetic spectra in ALMA receiver bands 6 through 9 for an isolated disk (left) and an irradiated disk (right).

Table 1. Column Densities and Integrated Line Strengths

Species	Column Density ^a				Transition	Frequency (GHz)	Line Strength ^b	
	(cm ⁻²)						(mJy km s ⁻¹)	
	Isolated		Irradiated				Isolated	Irradiated
	10 AU	100AU	10 AU	100AU				
<hr/>								
H	5.6(20)	1.3(19)	1.6(21)	2.2(21)
H ₂	2.6(24)	2.0(23)	2.1(24)	7.5(22)
C	2.3(17)	7.2(16)	4.7(17)	2.3(17)	³ P ₁ – ³ P ₀	492.161	...	22.8
					³ P ₂ – ³ P ₁	809.342	24.8	85.2
CO	2.7(20)	1.8(19)	2.3(20)	8.8(18)	1–0	115.271	14.5	31.2
					2–1	230.538	68.2	141
					3–2	345.796	163	326
					4–3	461.041	293	578
					6–5	691.473	599	1230
					7–6	806.652	734	1600
HCO ⁺	1.7(14)	4.8(13)	2.1(14)	3.0(14)	8–7	921.800	824	1970
					3–2	267.558	27.1	31.6
					4–3	356.734	54.1	86.9
					5–4	445.903	86.4	184
					7–6	624.209	150	545
					8–7	713.342	183	830
					9–8	802.456	225	1200

Table 1—Continued

Species	Column Density ^a				Transition	Frequency (GHz)	Line Strength ^b	
	(cm ⁻²)						(mJy km s ⁻¹)	
	Isolated		Irradiated				Isolated	Irradiated
	10 AU	100AU	10 AU	100AU				
CN					10–9	891.558	284	1670
	9.7(13)	8.0(13)	4.6(14)	5.5(14)	2 _{5/2} –1 _{3/2}	226.876	...	12.0
					3 _{5/2} –2 _{3/2}	340.031	...	32.9
					3 _{7/2} –2 _{5/2}	340.249	...	45.4
					4 _{7/2} –3 _{5/2}	453.390	14.0	83.2
					4 _{9/2} –3 _{7/2}	453.607	18.1	104
					6 _{11/2} –5 _{9/2}	680.047	32.4	221
					6 _{13/2} –5 _{11/2}	680.264	38.2	255
					7 _{13/2} –6 _{11/2}	793.336	37.7	278
					7 _{15/2} –6 _{13/2}	793.554	43.7	315
HCN					8 _{15/2} –7 _{13/2}	906.593	39.5	308
					8 _{17/2} –7 _{15/2}	906.811	44.7	345
	5.9(14)	2.1(13)	2.4(14)	1.0(14)	3–2	265.886	12.4	30.1
					4–3	354.505	27.1	71.9
					5–4	443.116	44.9	129
				7–6	620.304	80.2	251	
				8–7	708.877	98.0	295	

Table 1—Continued

Species	Column Density ^a				Transition	Frequency (GHz)	Line Strength ^b	
	(cm ⁻²)						(mJy km s ⁻¹)	
	Isolated		Irradiated				Isolated	Irradiated
	10 AU	100AU	10 AU	100AU				
					9–8	797.433	120	316
					10–9	885.971	149	313
CS	2.7(13)	1.5(13)	1.2(15)	2.0(13)	7–6	342.883	...	10.8
					8–7	391.847	...	14.2
					9–8	440.803	...	17.3
					10–9	489.751	...	19.6
					13–12	636.532	...	20.2
					14–13	685.436	...	18.5
					17–16	832.062	...	11.3
C ₂ H	7.7(13)	1.4(13)	2.3(14)	8.4(13)
H ₂ CO	8.1(11)	1.4(12)	9.3(11)	1.6(12)
N ₂ H ⁺	6.7(10)	3.1(11)	7.0(09)	8.9(09)
H ₂ O	8.4(16)	2.6(15)	1.2(16)	1.5(16)
OH	2.2(16)	5.2(14)	3.5(16)	4.9(16)
CO ₂	1.3(16)	2.7(16)	2.4(19)	1.4(17)
C ₂ H ₂	2.7(14)	3.0(13)	2.8(13)	1.2(13)

^a $a(b) = a \times 10^b$.

^b Listed line strengths are restricted to >10 mJy km⁻¹.